Eur. J. Mech., B/Fluids, **17,** n° 2, 187-203, 1998

Axisymmetric Stokes drag on hollow cylinders: Computation and comparison with experiment

R. P. ROGER * and P. D. WEIDMAN ** [1]

ABSTRACT. – The Beads-on-a-Shell (BoS) numerical technique for determining the Stokes drag on an object translating in an infinite fluid is applied to the class of finite rigid hollow cylinders with aspect ratio $0 \leq L/D \leq 20$ and inner-to-outer radius ratios $0 \leq R_i/R \leq 1.0$. Agreement with the Stokes drag measurements on hollow cylinders in the range $L/D < 4$ and $0.0 \leq R_i/R \leq 0.95$ reported by (Lasso and Weidman, 1986) is very good except at the extreme upper limits of L/D and R_i/R. The discrepancy is attributed to a breakdown of the *ad hoc* correction procedure adopted to account for wall interference and inertial effects on the measurements when the cylinders are long and thin. The BoS scheme was first tested by computing the Stokes drag and comparing with published analytical results for the axial translation of a solid cylinder, a cylindrical shell, and a spherical shell with opposing polar caps removed. © Elsevier, Paris.

1. Introduction

The Beads-on-a-Shell (BoS) technique for computing the Stokes flow drag may be applied to many geometrical shapes, including simply- and multiply-connected bodies. The method makes use of the pairwise hydrodynamic interaction between two small spheres of fixed separation in an unbounded fluid moving with constant velocity at infinity. The interaction is calculated as the force approximated by an array of small spheres distributed with their centers on the geometric surface of the object. The drag on the array is computed by appropriately summing all pairwise interactions. Using an increasing number of spheres of decreasing size, the drag on the body is obtained as an extrapolation to zero dimensionless sphere size. This extrapolation procedure has the distinct advantage that it can handle sharp geometric corners with ease. Moreover, it has previously been shown capable of reproducing exact analytical results for the Stokes drag of the following bodies in uniform translation: the sphere, the cardioid, the toroid (heretofore unpublished), the double convex lens, full and annular flat disks, and certain finite length solid cylinders.

It is our understanding that the Stokes drag has not yet been computed for hollow cylinders. We undertake this task to compare with the existing measurements of (Lasso and Weidman, 1986). In that study an *ad hoc* correction procedure to account for unavoidable inertial and sidewall blockage effects was introduced. An additional benefit of the present study is to evaluate the range of usefulness of that correction procedure. Moreover, we report new laboratory measurements of the Stokes drag on very thin-walled cylinders approximating a cylindrical shell to compare with asymptotic results reported by (Price, 1985). Finally, the Stokes drag on a spherical shell with end caps symmetrically removed fore and aft is determined to compare with the analysis of (Davis, 1985) and it is shown how this geometry becomes an approximation to the cylindrical shell when the conical angle of the removed end caps approaches 90 degrees.

* The Johns Hopkins University, Applied Physics Laboratory, Laurel, MD 20723-6099 USA.
** Laboratoire d'Hydrodynamique, École Polytechnique, 91128 Palaiseau Cedex, France.
[1] Permanent address: Department of Mechanical Engineering. University of Colorado, Boulder, CO 80309 USA.

0997-7546/98/02/© Elsevier, Paris

Consider then axisymmetric uniform zero Reynolds number flow over the hollow cylinder illustrated in Figure 1. The fluid extends to infinity in all directions and the Reynolds number, $\mathrm{Re} = \rho UD/\mu$, approaches zero, where U is the uniform translation velocity of the cylinder along its axis, D is the outer diameter, D_i its inner diameter, and ρ and μ are the density and viscosity of the homogeneous fluid, respectively. The multi-connected geometry of the hollow cylinder, consisting of a finite length cylinder with a concentric axial hole, is completely specified by its length L, its outer radius $R = D/2$, and its inner radius $R_i = D_i/2$. Thus the dimensionless geometrical parameters are the radius ratio R_i/R and the aspect ratio L/D. Limiting cases of these parameters specify configurations of interest which have been previously studied, namely

(a)	$R_i/R = 0$	finite length solid cylinder
(b)	$L/D = 0$	annular disk of zero thickness
(c)	$R_i/R = 1$	finite length cylindrical shell
(d)	$R_i/R = 0,\ L/D = 0$	full disk of zero thickness.

An historical perspective may be gleaned from the following literature compiled on the subject. Case (a) has been studied analytically by (Burgers, 1938), (Broersma, 1960), (Cox, 1970), (Batchelor, 1970), (Keller and Rubinov, 1976) and (Russel *et al.*, 1977), numerically by (Gluckman *et al.*, 1972), (Youngren and Acrivos, 1975) and (Swanson *et al.*, 1978), and experiments have been reported by (Heiss and Coull, 1952), (Blumberg and Mohr, 1968), (de Mestre, 1973) and (Ui *et al.*, 1984). Case (b) has been studied numerically and experimentally by (Roger and Hussey, 1982) and analytically by (Davis, 1991). Case (c) has been studied analytically by (Price, 1985). Case (d) has been studied analytically by (Sampson, 1981) and numerically by (Roger and Hussey, 1982). The only available study for cylinders at nonzero values of R_i/R with nonzero values of L/D appears to be the measurements of (Lasso and Weidman, 1986).

Our goal is to compute the Stokes drag for hollow cylinders in order to compare with the above-mentioned measurements reported over the range $0 \leq R_i/R \leq 0.875$ and $0.25 \leq L/D \leq 4$, and with measurements at $R_i/R = 0.95$ over the same range of aspect ratios reported here for the first time. The outline of the presentation is a follows. Salient features of the BoS method used in this study are given in § 2. Code-testing is carried out in § 3 in which, *inter alia*, new computations for the spherical shell with symmetrically removed end caps are given. Also in § 3 BoS results for a solid cylinder are reported and compared with the Stokeslet patch

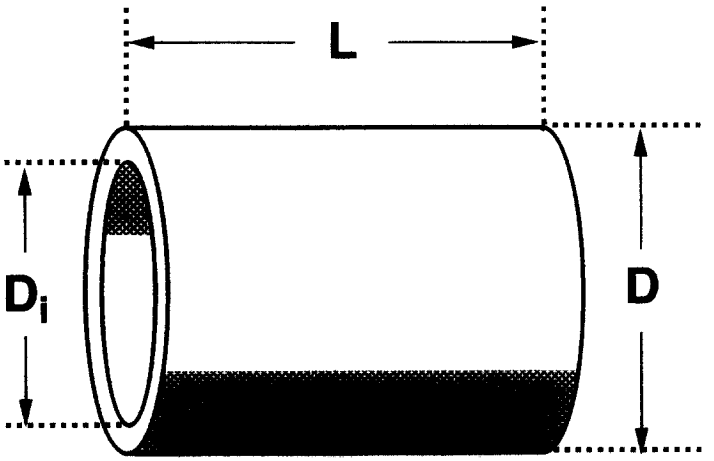

Fig. 1. – Hollow cylinder configuration.

numerical method used by (Youngren and Acrivos, 1975). The hollow cylinder computations are presented § 4 and concluding remarks are given in § 5.

2. The numerical method

The BoS method is based on the hydrodynamical tensor for the interaction between point forces developed by (Oseen, 1927) and (Burgers, 1938). This tensor provides the fluid velocity perturbation at the site of one point force due to the presence of the other. The pairwise interaction provides the resulting Stokes drag force on the two-point-force configuartion. The approach is to transform the interaction tensor between two point forces into an interaction tensor between two small spherical distributions of the point forces, or two small spheres. Since the Stokes equations are linear, the force on an array of small spheres, or beads, can be determined by summing the pairwise interaction among the spheres in the array.

We briefly introduce the mathematical formulation of these ideas for general translation of a point force and then specialize it to our application for motion along a principle axis. For translation of a point force located at the origin of coordinates in the Stokes limit, the velocity perturbation at r is give by

$$\mathbf{v}' = \overline{\overline{T}}_0(\mathbf{r})\,\mathbf{F} \tag{1}$$

where $\overline{\overline{T}}_0(\mathbf{r})$ is the Oseen hydrodynamic interaction tensor

$$\overline{\overline{T}}_0(\mathbf{r}) = \frac{1}{8\pi\mu r}\left(\overline{\overline{I}} + \frac{\mathbf{rr}}{r^2}\right) \tag{2}$$

with μ as previously defined and $\overline{\overline{I}}$ is the unit tensor. The point force is then distributed uniformly over a small spherical surface of radius a with center at the origin by averaging $\overline{\overline{T}}_0(\mathbf{r} - a\mathbf{e}_r)$ over the spherical surface, where $\mathbf{e}_r$ is the unit vector in the radial direction. The result is the modified tensor (Yamakawa, 1970)

$$\overline{\overline{T}}_0(\mathbf{r}) = \frac{1}{8\pi\mu r}\left[\left(1 + \frac{a^2}{3r^2}\right)\overline{\overline{I}} + \left(1 - \frac{a^2}{r^2}\right)\frac{\mathbf{rr}}{r^2}\right] \tag{3}$$

which replaces $\overline{\overline{T}}_0(\mathbf{r})$ in Eq. (1). If $\mathbf{F}$ is identified with the Stokes drag on a sphere of radius a translating with velocity $\mathbf{U}$ in an unbounded fluid, then evaluation of $\overline{\overline{T}}_0(\mathbf{r}) \cdot \mathbf{F}$ yields the Stokes velocity distribution around the sphere. This implies that a sphere translating in an unbounded fluid may be replaced by a uniform spherical surface distribution of force translating in the fluid and having magnitude equal to the frictional force exerted by the sphere on the fluid. Such a spherical distribution is referred to as a "bead".

The interaction of two such beads with fixed relative positions may be obtained as follows. Position the first bead at $\mathbf{r}_1$ and the second at $\mathbf{r}_2$, both translating with the body-fixed coordinate system at steady velocity $\mathbf{U}$ through the fluid. The force exerted on the fluid by the first is identified as

$$\mathbf{F}_1 = \zeta(\mathbf{U} - \mathbf{v}_1') \tag{4}$$

where $\zeta = 6\pi\mu a$ is the Stokes friction coefficient for each bead, and $\mathbf{v}_1'$ is the perturbation due to bead 2 at the surface of bead 1. Now $\mathbf{v}_1'$ is calculated by averaging the Oseen tensor over both spherical surfaces, providing a new interaction tensor which contains a first order correction to the Oseen result (Rotne and Prager, 1969; Yamahawa, 1970), *viz.*

$$\overline{\overline{T}}_{12} = \frac{1}{8\pi\mu r_{12}}\left[\left(1 + \frac{2a^2}{3r_{12}^2}\right)\overline{\overline{I}} + \left(1 - \frac{2a^2}{r_{12}^2}\right)\frac{\mathbf{r}_{12}\,\mathbf{r}_{12}}{r_{12}^2}\right]. \tag{5}$$

This result is sufficient for two equal radii beads that do not overlap. In some instaces it is convenient to use overlapping spheres of equal radii in which case the result

$$\overline{\overline{T}}_{12} = \frac{1}{6\pi\mu r_{12}}\left[\left(1 - \frac{9r_{12}}{32a}\right)\overline{\overline{I}} + \frac{\mathbf{r}_{12}\,\mathbf{r}_{12}}{32ar_{12}}\right]. \tag{6}$$

reported by (Rotne and Prager, 1969) is employed. In special cases that warrant a construction using touching spheres of unequal radii, the Oseen tensor found by (de la Torre and Bloomfield, 1977) is used. In every instance the interaction tensor is independent of $\mathbf{U}$ and depends only on the sphere radii and their relative positions $\mathbf{r}_{12}$. In general, the force exerted at $\mathbf{r}_1$, calculated from Eqs. (4) and (1), is given by

$$\mathbf{F}_1 = \zeta_1\,\mathbf{U} - \zeta_1\,\overline{\overline{T}}_{12}\,\mathbf{F}_2, \tag{7}$$

where ζ_1 is associated with a_1. We now construct a rigid assembly by N such beads translating through a quiescent fluid. The force on the fluid at the site of the i^{th} bead, equal in magnitude and opposite in direction to the drag force on that bead, is

$$\mathbf{F}_i = \zeta_i\,\mathbf{U} - \sum_{j=1}^{N} \zeta_i\,\overline{\overline{T}}_{ij}\,\mathbf{F}_j, \qquad (i \neq j) \tag{8}$$

and this may be suitably rearranged for calculation of the drag on the entire assembly, *viz.*

$$\sum_{j=1}^{N} \delta_{ij}\,\mathbf{F}_i + \sum_{j=1}^{N} \zeta_i\,\overline{\overline{T}}_{ij}\,\mathbf{F}_j = \zeta_i\,\mathbf{U}, \qquad (i \neq j). \tag{9}$$

There are N such equations, one for each bead in the assembly, each having three components. This system of equations may then be written

$$\mathcal{M}\mathcal{F} = 6\pi\mu\mathcal{U}, \tag{10}$$

where $\mathcal{M}$ is a $3N \times 3N$ blocks matrix containing 3×3 $\mathcal{M}_{ij}$ and $\mathcal{F}$ and $\mathcal{U}$ are $3N \times 1$ column vectors. The force components on each bead in the assembly can be found by inverting $\mathcal{M}$ and solving

$$\mathcal{M}\mathcal{F} = 6\pi\mu\,\mathcal{M}^{-1}\mathcal{U}. \tag{11}$$

The components of the net force on the entire array of beads are the sums of the respective components of each bead. Clearly, the solution requires the inversion of $3N \times 3N$ matrix.

For our application, however, two simplifications can be made. First, because we consider only translation along a principle axis, the body will experience a force only along this direction (Happel and Brenner, 1973). Then $\mathcal{M}$ reduces to an $N \times N$ matrix, $\mathcal{F}$ and $\mathcal{U}$ are $N \times 1$ column vectors and, for translation along the x-axis, Eq. (10) takes the form

$$\begin{pmatrix} a_1^{-1} & \mathcal{M}_{12}^{xx} & \mathcal{M}_{13}^{xx} & \cdot & \cdot & \mathcal{M}_{1N}^{xx} \\ \mathcal{M}_{21}^{xx} & a_2^{-1} & \mathcal{M}_{23}^{xx} & \cdot & \cdot & \mathcal{M}_{2N}^{xx} \\ \cdot & \cdot & \cdot & \cdot & \cdot & \cdot \\ \cdot & \cdot & \cdot & \cdot & \cdot & \cdot \\ \mathcal{M}_{N1}^{xx} & \mathcal{M}_{N2}^{xx} & \mathcal{M}_{N3}^{xx} & \cdot & \cdot & a_N^{-1} \end{pmatrix} \begin{pmatrix} F_1^x \\ F_2^x \\ \cdot \\ \cdot \\ F_N^x \end{pmatrix} = 6\pi\mu \begin{pmatrix} 1 \\ 1 \\ \cdot \\ \cdot \\ 1 \end{pmatrix} \tag{12}$$

where $\mathcal{M}_{ij}^{xx} = 6\pi\mu T_{ij}^{xx}$ and the superscripts refer to the xx-component of the tensor $\overline{\overline{T}}_{ij}$. Second, our geometries have axial symmetry. Then, choosing the beads to be of equal size and arranged in concentric rings about the symmetry axis (the x-axis), the force on each bead in a ring is the same. Then it is possible to sum over each ring *before* inversion and $\mathcal{M}$ reduces of the much smaller $N_r \times N_r$ matrix $\mathcal{M}'$, where N_r is the total number of rings in the assembly. The elements of $\mathcal{M}'$ are given by

$$\mathcal{M}'_{ij} = N_j \sum_{k=1}^{N_j} \mathcal{M}_{i_1 k}^{xx} \tag{13}$$

where N_j is the number of beads in ring j, i refers to the i-th ring, i_1 refers to bead 1 in ring i, and $\mathcal{M}_{ii}^{xx} = 1/a_i$.

Additional details of the method can be found in review articles by (Teller *et al.*, 1979) and (de la Torre and Bloomfield, 1981). The BoS technique yields accurate results only in extrapolated limit of infinitely small beads. Another technique, the multipole expansion method, was first systematically studied by (Ladd, 1988, 1989, 1990). (Chichocki *et al.*, 1994) obtained increased accuracy for finite arrays of spheres of different radii using a modified multiple expansion technique. (Cichocki and Hinsen, 1995) applied that technique to calculate the Stokes drag for conglomerates composed of n-touching spheres of equal radii in order to compare with the experimental measurements of (Lasso and Weidman, 1986). They found agreement with the measurements to better than 3% for conglomerates composed of 2, 3, 5, 13, 55, 57, 147, 153 and 167 spheres assembled in specified symmetrical hcp or fcp packing arrangements.

3. Code testing

Objects are modeled by distributing the spheres with their centers on the actual geometrical surface of the object. For the hollow cylinder, this distribution is characterized by the ratio a/R of bead radius to outer cylinder radius. Figure 2 provides a visualization of the bead arrays assembled for two values of a/R for a typical hollow cylinder. Equations are established for the end faces and one each for the inner and outer surfaces. The equations are designed so neighboring beads at least touch. However, since a/R varies continuously but bead numbers can only vary in units of a whole bead, there is usually some overlapping. As the interaction matrix is being constructed, pairwise center-to-center distances are checked, and the appropriate tensor (5) or (6) is used to compute the pairwise interaction. Furthermore, the inner and outer corners of the hollow cylinders have been modeled by placing a ring of beads exactly at the corner; *i.e.* the centers of the beads in the "corner ring" lie on the geometrical corner. (Ui *et al.*, 1984) have studied the problem of corner formation in the BoS technique. They demonstrated that even if the corner is rounded using overlapping beads, the extrapolation to an infinite numgber of beads gives the same Stokes drag as for touching beads; however, the approach to the extrapolated result follows different curves. A graphical representation of the extrapolation of BoS results to $a/R = 0$ for a unit aspect ratio hollow cylinder at five different radius ratios is given in Figure 3.

In applying the BoS method, the solution is obtained by inverting an $N_r \times N_r$ matrix, where N_r is the number or bead rings (*cf. Fig.* 2). In this study a Gauss-Seidel iteration procedure was employed. For each of the arrays, a FORTRAN program was devised to construct the matrix and perform the matrix inversion. Computations were carried out on a Silicon Graphics Crimson workstation. All results were obtained using a convergence criterion that successive iterations differ by less that 1.0×10^{-5} percent.

To establish the accuracy of the BoS method we have applied it to a variety of solid shapes for which exact analytical solutions exist. The particle shapes chosen are the sphere, the disk of zero thickness, the double convex lens (Wakiya, 1980), the cardioid (Richardson, 1977), and the torus (Majundar and O'Neil, 1977; Hussey *et al.*, 1982). Extrapolated dimensionless drags for these cases are listed in Table I. Comparison with the analytical

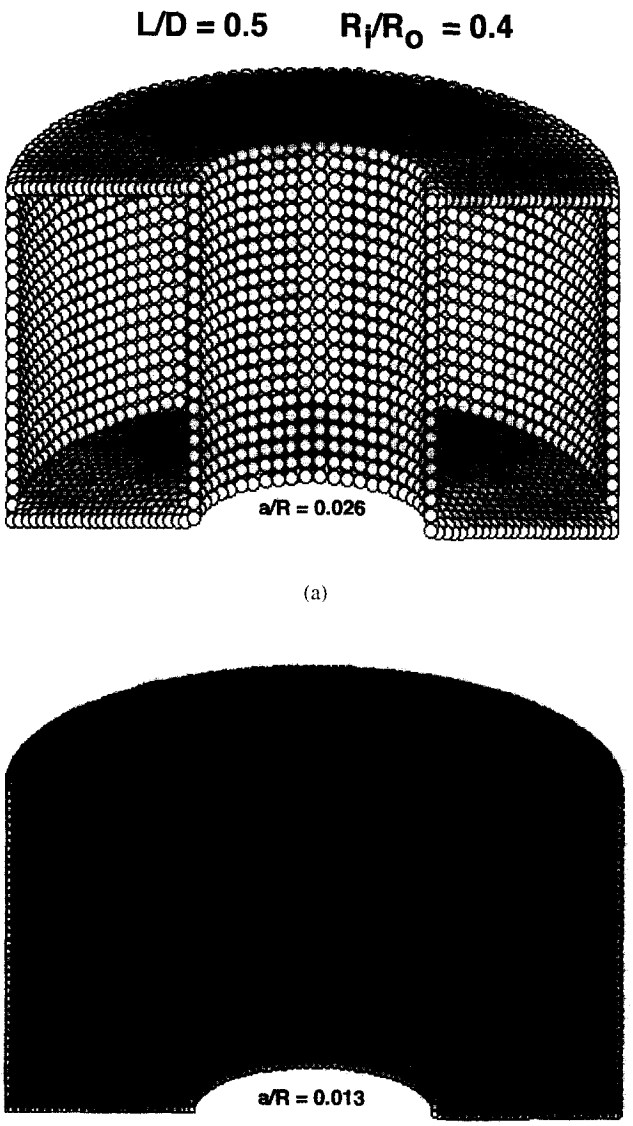

Fig. 2. – Cut-away view showing BoS constructions for different bead sizes: (a) $a/R = 0.026$ and (b) $a/R = 0.013$.

result for each geometry is made by presenting the percent difference relative to the analytical value. For these shapes the BoS technique yields the exact result to better than 0.1%.

Three analytical results are available for thin-walled multi-connected bodies. An expression for the drag of an annular disk of zero thickness, limiting case (b), was reported by (Davis, 1991). Our numerical results are compared with his predictions in tabular form in Table II and in graphical form in Figure 4. (Davis, 1985) has also reported calculations for a spherical shell with symmetrical front and rear conical sections removed. We have computed the Stokes drag for this body over a wide range of angles of the removed end caps. The comparison of these calculations with the results of (Davis, 1985) are given in tabular form in Table III and

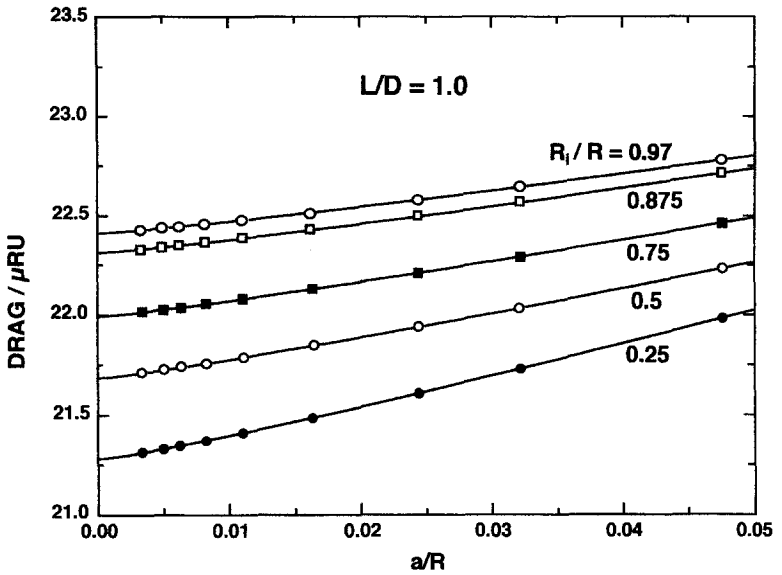

Fig. 3. – Plot showing the extrapolation of non-dimensional drag to zero bead size for a hollow cylinder at different radius ratios.

TABLE I. – Computations of the normalized drag $\mathrm{Drag}/\mu RU$ for simple geometrical shapes; * axial translation, ** translation perpendicular to axis, $^{+}$15 degree half angle, $^{\dagger}R/r = 10$, $^{\dagger\dagger}R/r = 20$ where R is the torus radius and r is the torus half width.

	$\mathrm{Drag}/\mu RU$		
Object	BoS method	Exact analytical	% difference
Zero thickness disk*	16.0002	16.00000	0.001
Zero thickness disk**	10.6677	32 π/3	0.010
30° lens*$^{+}$	16.0034	16.00512	0.011
120° lens*	16.5970	16.60656	0.057
sphere*	18.8499	6 π	0.002
cardiod*	18.5824	18.58480	0.013
torus*†	14.7846	14.78390	0.063
torus*††	13.5096	13.51136	0.013

in graphical form in Figure 5. It is clear that the BoS Stokes drag for these axisymmetric geometries are in excellent agreement with Davis's analytical results.

A cylindrical shell of finite length belongs to the family of multi-connected bodies corresponding to limiting case (c). The asymptotic drag for this geometry, valid for $L/D \ll 1$, was reported by (Price, 1985). Our results for the BoS drag are compared with Price's computed values both in Table IV and in Figure 6. Also included in Figure 6 are the results of (Davis, 1985) for the spherical shell with end caps removed, since for large polar cap angles this shape closely resembles a cylindrical shell with small L/D. For the results of (Davis, 1985), the aspect ratio is equated to $\cos\alpha$, where α is the polar cap angle as shown in the inset of Figure 5.

The results found by (Price, 1985) apply asymptotically as $L/D \to 0$. In the range $L/D < 0.1$, the BoS predictions are consistent with those of (Price, 1985), while above this aspect ratio the results exhibit a slow divergence. It is interesting to note, however, that below $L/D \sim 0.2$ the drag predictions for the open spherical shell and the cylindrical shell are almost indistinguishable. For small L/D, the asymptotic behavior for the dimensionless drag may be represented by the empirical equation

$$\mathcal{D} \equiv \mathrm{Drag}/16\,\mu RU = (\pi^2/2)\,[\ln(8\,D/L) + 0.5]^{-1}. \tag{14}$$

TABLE II. – Computations of the normalized drag $\mathrm{Drag}/16\,\mu\,RU$ for an annular disc of vanishing thickness.

Radius ratio	$\mathrm{Drag}/16\,\mu\,RU$	
	Davis	BoS
0.0000		1.0000
0.2500		0.9975
0.5000	0.9810	0.9806
0.6667	0.9494	
0.7500		0.9212
0.8000	0.8977	
0.8333	0.8778	
0.8750		0.8456
0.8889	0.8329	
0.9167	0.8015	
0.9600	0.7259	
0.9700		0.7019
0.9800	0.6634	
0.9900	0.6094	
0.9950		0.5619

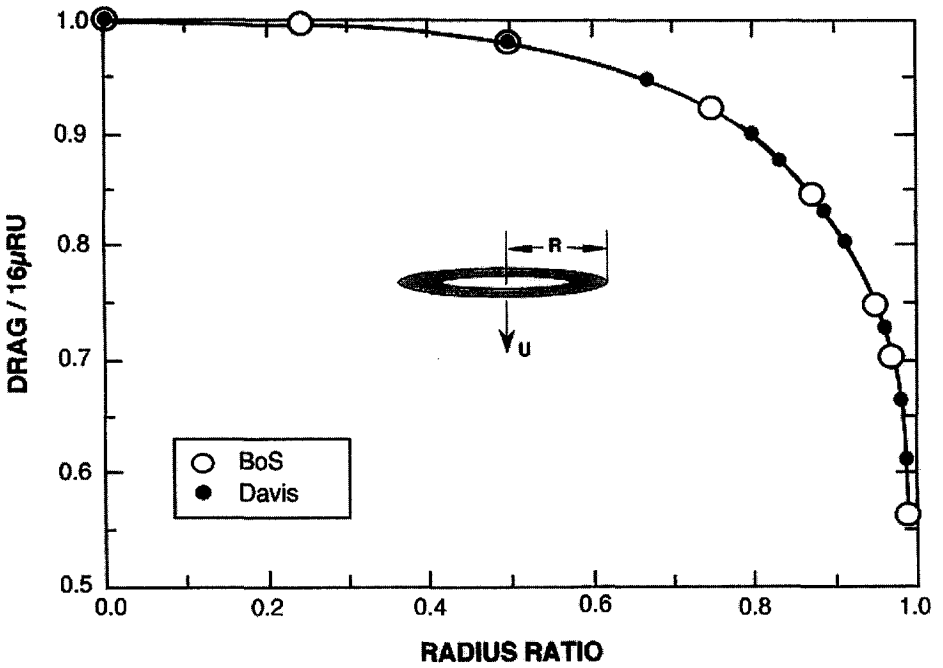

Fig. 4. – Dimensionless drag for an annular disc of zero aspect ratio as a function of the radius ratio.

This result provided by (Davis, 1985), with streamwise arc angle $\pi - 2\,\alpha$ replaced by $2\,L/D$, is identical to the asymptotic formula given by (Price, 1985), and is included as the solid line in Figure 6.

It is instructive to compare calculations for both hollow and solid cylinders in the extreme limits of large and small L/D. The BoS predictions over a wide range of aspect ratios are shown in Figure 7; here the drag is normalized with the exact value for a disk of zero thickness, $16\,\mu\,RU$, found by (Sampson, 1891). An expanded view of this presentation for $L/D > 1$ is given in Figure 8.

TABLE III. – Computations of the normalized drag $\mathrm{Drag}/6\pi\mu RU$ for a hollow spherical shell with front and rear cap elements removed.

Cap angle (deg)	$\mathrm{Drag}/6\pi\mu RU$	
	Davis	BoS
0		18.850
10		18.842
20	18.787	
30	18.644	18.640
40	18.371	
50	17.918	
60	17.212	17.160
66.67	16.539	
72	15.804	
75	15.312	
80	14.273	14.240
85.71	12.431	
87.80	11.270	

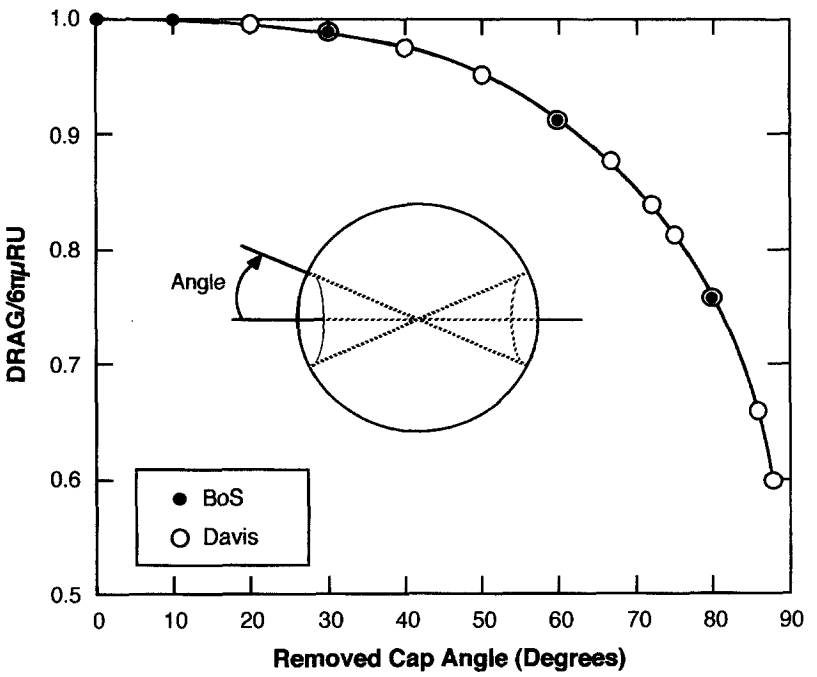

Fig. 5. – Dimensionless drag for a spherical shell with polar caps removed as a function of the cap opening angle.

BoS predictions performed by (Ui *et al.*, 1984) for solid cylinders moving axially have been compared with earlier numerical results reported by (Gluckman *et al.*, 1972) and (Youngren and Acrivos, 1975), the latter investigators using a method called Stokeslet patches. In that general method, the elements of the interaction tensor are evaluated by numerical integration over small patches distributed over the surface of a body. Accurate results are obtained using patches of sufficiently small size that the computed drag converges to a fixed value. This technique was shown to reproduce analytical results for spheroids. The sharp edge of the cylinder gives rise to a singular shear stress. Patches placed adjacent to the a corner on each bounding surface do not alter the integrity of the corner. Aspect ratios in the range $0.5 \leq L/D \leq 100$ were investigated by (Youngren and Acrivos, 1975) and their large aspect ratio results agreed well with those found using slender body theory

TABLE IV. – Computations of the normalized drag $\mathrm{Drag}/16\mu RU$ for a cylindrical shell and a spherical shell with end caps removed; †spherical shell with open end cap angle α; the length to diameter ratio is $\cos\alpha$.

	$\mathrm{Drag}/16\mu RU$		
L/D	BoS	Price	Davis†
0.00010	0.3788		
0.0010	0.4606		
0.01047	0.5931		
0.02618	0.6669		
0.03125		0.6816	
0.03833			0.7044
0.05235	0.7250		
0.0625		0.7544	
0.0748			0.7770
0.1250		0.8450	
0.13090	0.8506		
0.1763			0.8921
0.2500	0.9544	0.9622	
0.3090			0.9877
0.5000	1.1025	1.1219	1.0757
0.6428			1.1199
0.7660			1.1482
0.8660			1.1653
0.9397			1.1742
1.0000	1.3131	1.3519	
2.0000	1.6506		
3.0000	1.9475		
4.0000	2.2206		
5.2360	2.5397		
10.472	3.7281		
20.944	5.7688		

(Batchelor, 1970). Figure 9 provides a comparison of predictions for the solid cylinder translating along its axis using the BoS method, the Stokeslet patch method, and slender body theory. Also included in Figure 9 is a curve representing an empirical expression provided by Eq. 12 (Ui *et al.*, 1984) for values $L/D < 0.1$. The plot is presented in terms of the settling factor KS, defined as the ratio of the drag on a sphere with the same volume as the cylinder to that on the cylinder when both are exposed to the same uniform external flow (*cf.* Gluckman *et al.*, 1972). One may observe the following:

(i) for $L/D > 4.0$, the BoS and Stokeslet patch results are in essential agreement;

(ii) as $L/D \rightarrow 100$, the Stokeslet patch results and slender body theory become equivalent;

(iii) for $L/D < 4.0$, the BoS and Stokeslet patch results increasingly diverge as $L/D \rightarrow 0$.

This last observation is made clearer in Figure 10, which provides the aspect ratio on a linear scale and restricts the presentation to L/D values between zero (flat disk) and unity. Table V gives a tabulation of the points plotted in Figures 9 and 10. The corner becomes increasingly more important as $L/D \rightarrow 0$. In this region the results of (Youngren and Acrivos, 1985) give an upper bound to the dimensionless cylinder drag, but it appears that smaller Stokeslet patches than those employed will be necessary to produce results that extrapolate to the known analytical result for a circular wafer. It is evident, however, that sufficiently small beads have been used for BoS calculations to converge uniformly to the exact drag limit of (Sampson, 1891) at $L/D = 0$.

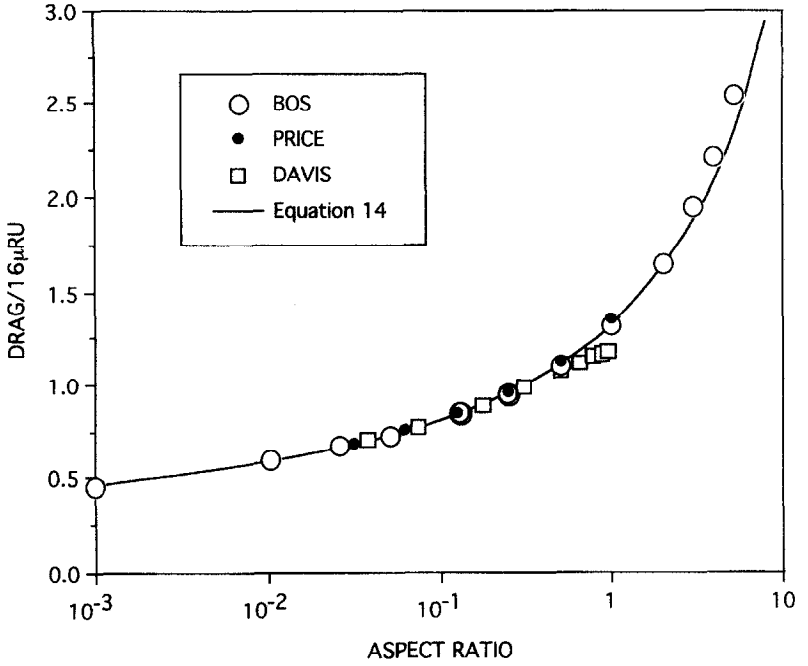

Fig. 6. – Dimensionless drag for open cylindrical shells as a function of aspect ratio; values for open spherical shells are included for comparison.

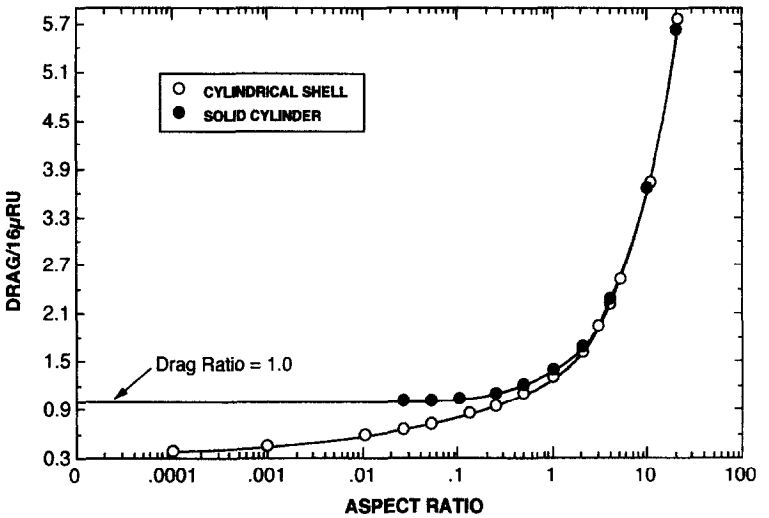

Fig. 7. – A comparison of the dimensionless drag of cylindrical shells and solid cylinders as a function of aspect ratio.

4. Hollow cylinder results

Normalized drags for hollow cylinders computed using the BoS technique over the range of radius ratios $0 \leq R_i/R \leq 1$ and aspect ratios $0 \leq L/D \leq 4$ are listed in Table VI. Analytical solutions for the zero Reynolds number drag of solid and hollow cylinders falling along their axis of symmetry are not available. The best experimental measurements for solid cyinders ($R_i/R = 0$) to date appear to be those of (Heiss and Coull, 1952) who tested a series of geometrically similar cylinders and extrapolated measurements to zero Reynolds number

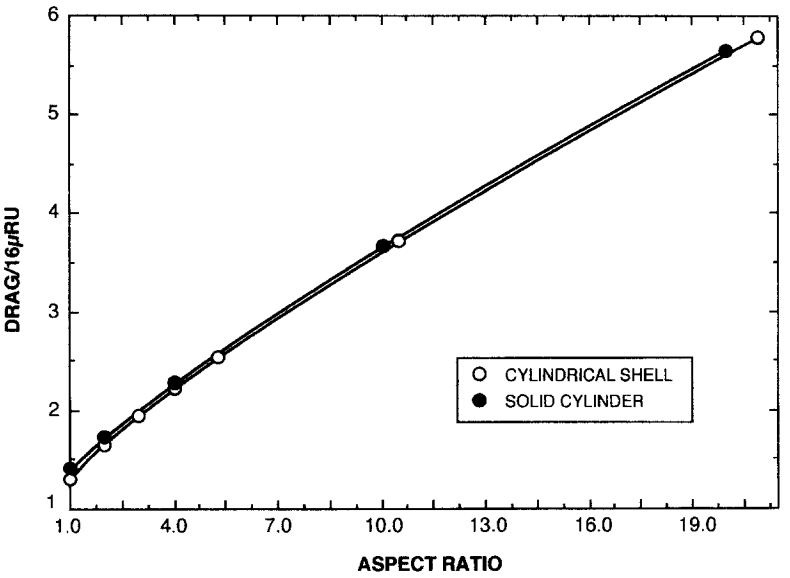

Fig. 8. – A comparison of the dimensionless drag of cylindrical shells and solid cylinders in the range of moderate to large aspect ratio.

in order to obtain the drag coefficient for inertialess flow in an unbounded fluid. Measurements of the Stokes drag of hollow cylinders were reported by (Lasso and Weidman, 1986) over the range of geometric parameters $0 \leq R_i/R \leq 0.875$ and $0.25 \leq L/D \leq 4$. They used an *ad hoc* correction procedure outlined in § III of their paper to correct for inertial and wall interference effects in their finite tank of square section. This procedure reduces near-axisymmetric test objects to "equivalent" spheres falling along the axis of an equivalent tank of circular section which then correspond to the well-known measurements of Sutterby (1973) for the low Reynolds number drag of spheres translating along the central axis of a cylindrical tank. The good agreement in drag measurements for solid cylinders constructed of two different plastic materials (ABS of density 1.037 g/cm^3 and Delrin of density 1.42 g/cm^3) with the computations of (Youngren and Acrivos, 1972) showed that the *ad hoc* correction procedure worked well, at least for the solid cylinders of moderate aspect ratio that were tested.

In this study we report additional experiments undertaken in an attempt to measure the stokes drag of finite aspect ratio cylindricall shells. Seven cylinders with nominal aspect ratios $1 \leq L/D \leq 4$ were constructed at the largest radius ratio which could be accurately machined from ABS plastic stock. The actual aspect ratios were somewhat smaller that the nominal values originally sought, and the measured values of L/D are listed in Table VII. Separate micrometer and buoyancy-inferred measurements of the radius ratio for all cylinders gave average values $R_i/R = 0.945$ and $R_i/R = 0.950$, for the respective methods. Since the buoyancy-inferred measurement of test model volumes is generally more accurate than direct measurement, we take $R_i/R = 0.950$ as the nominal radius ratio. The measured volume V and hydrodynamic drag D (weight submerged in the test fluid) of each hollow cylinder are listed in Table VII. A detailed description of the experimental facility and the measurement procedure is given in § II of (Lasso and Weidman, 1986). Since the silicone oil used in the present experiment was the same as that used previously, the temperature dependence of density and viscosity given by Eqs. (6) and (7) of (Lasso and Weidman, 1986) are applicable here. The only difference is that the separation distance between the laser beams was slightly different from the original setup, it now being 29.69 cm. Table VII gives the measured values of terminal settling speed U_m, blockage ratio d/d_e, Reynolds number Re, Sutterby correction factor $K = U/U_m$, Stokes settling speed ratio $KS = U/U_r$, test fluid temperature T, and the average tilt angle ϕ of the cylinders from vertical; here U is the terminal Stokes settling speed in an unbounded fluid and U_r is the Stokes settling speed of a reference sphere with mass and volume equal to that of the test object.

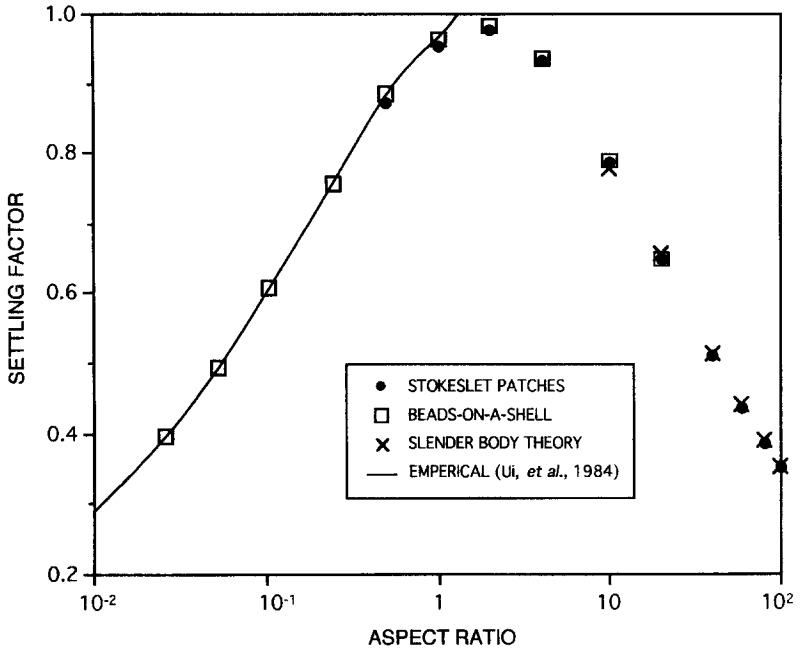

Fig. 9. – Solid cylinder settling factors computed by the BoS method and by Stokeslet patches compared with slender body theory results as a function of aspect ratio.

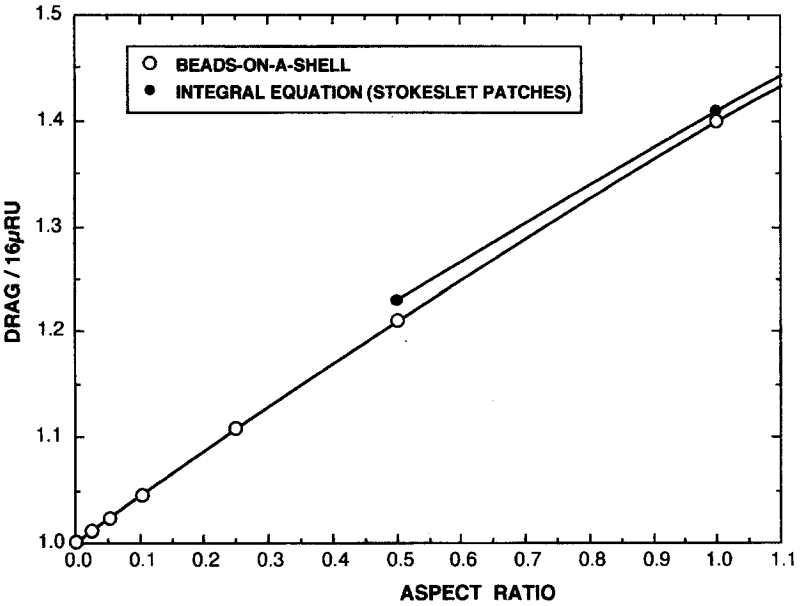

Fig. 10. – A comparison of normalized drag for solid cylinders computed by the BoS method and by Stokeslet patches at small aspect ratios.

Numerical and experimental results for the dimensionless drag $D/\mu RU$ variation with aspect ratio are plotted in Figure 11 with the radius ratio as a parameter. The data for $R_i/R = 0.25$, 0.50, 0.75 and 0.875 represent the average values of Lasso and Weidman's measurements for geometrically similar ABS and Delrin cylinders; the data for $R_i/R = 0.95$ are the new measurements for the thin-walled cylinders made of ABS. Figure 12

TABLE V. – Computations of the normalized drag $\mathrm{Drag}/6\mu RU$ for a solid cylinder of varying aspect ratio.

L/D	Stokeslet patches	$\mathrm{Drag}/\mu RU$	
		BoS	Slender body theory
0.026		0.396	
0.052		0.493	
0.105		0.608	
0.250		0.757	
0.500	0.873	0.884	
1.000	0.954	0.964	
2.000	0.977	0.983	
4.000	0.932	0.936	
10.00	0.788	0.790	0.781
20.00	0.649	0.649	0.658
40.00	0.510		0.518
60.00	0.435		0.441
80.00	0.387		0.391
100.0	0.351		0.354

TABLE VI. – Computations of the normalized drag $\mathrm{Drag}/16\mu RU$ for hollow cylinders as a function of radius ratio R_i/R and aspect ratio L/D.

L/D	R_i/R							
	0.0	0.25	0.5	0.75	0.875	0.95	0.97	1.0
0.00	1.000	0.9975	0.9806	0.9213	0.8456	0.7475	0.7019	0.000
0.25	1.108	1.108	1.100	1.071	1.037	1.001	0.9863	0.9544
0.50	1.211	1.210	1.205	1.184	1.159	1.134	1.124	1.103
1.00	1.400	1.400	1.394	1.374	1.354	1.336	1.329	1.313
2.00	1.728	1.728	1.722	1.704	1.686	1.671	1.664	1.651
3.00	2.019	2.019	2.014	1.997	1.981	1.966	1.961	1.948
4.00	2.288	2.288	2.283	2.268	2.253	2.239	2.233	2.221

TABLE VII. – Experimental data for the experiments on thin-walled hollow cylinders.

L/D	V (cm^3)	Drag (dyne)	U_m (cm/sec)	d/d_c	Re	K	KS	T (°C)	ϕ (deg)
0.957	0.1752	10.67	0.0717	0.019	0.0097	1.038	0.468	22.82	2
1.427	0.2656	16.11	0.0968	0.021	0.0151	1.041	0.482	22.90	5
1.905	0.3524	21.54	0.1155	0.022	0.0204	1.044	0.474	22.90	4
2.379	0.4254	25.80	0.1267	0.024	0.0245	1.048	0.464	22.82	2
2.857	0.5386	32.71	0.1479	0.025	0.0313	1.052	0.464	22.82	2
3.333	0.6050	36.78	0.1565	0.027	0.0352	1.056	0.455	22.82	1
3.810	0.6845	41.70	0.1647	0.029	0.0400	1.060	0.442	22.82	0

shows an alternative presentation of results in the form of dimensionless drag *versus* radius ratio with aspect ratio as a parameter. In Figure 12 the values of drag measured at $L/D = 0.957$, 1.905, 2.857, and 3.810 have respectively been adjusted to the nominal values $L/D = 1.0$, 2.0, 3.0, and 4.0 using the formula

$$D = D_0 + \left.\frac{\partial D}{\partial A}\right|_{A=A_0} (A - A_0) \tag{15}$$

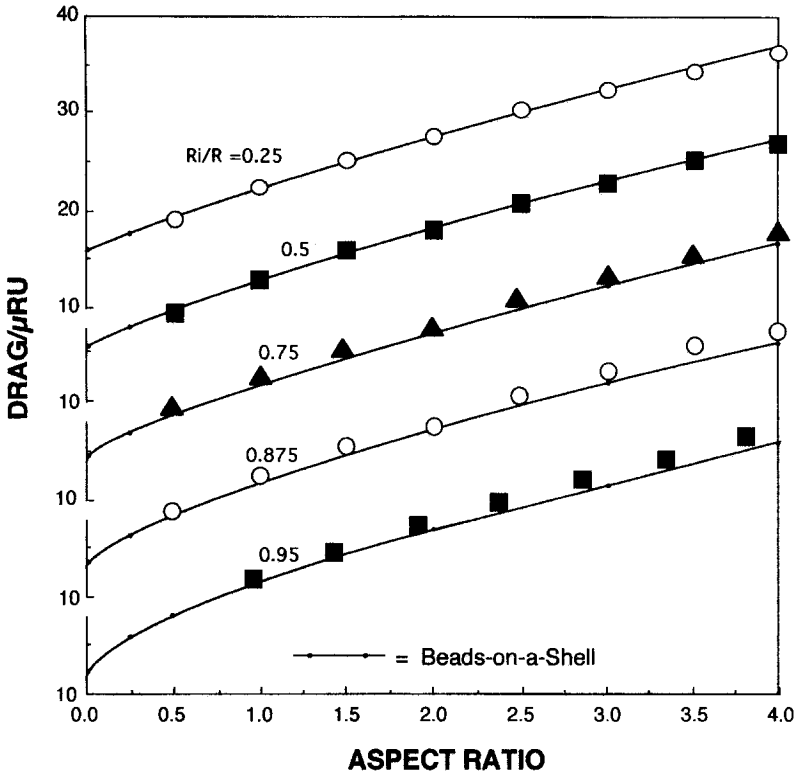

Fig. 11. – Measured and computed values of the normalized drag for hollow cylinders as a function of aspect ratio with R_i/R as a parameter.

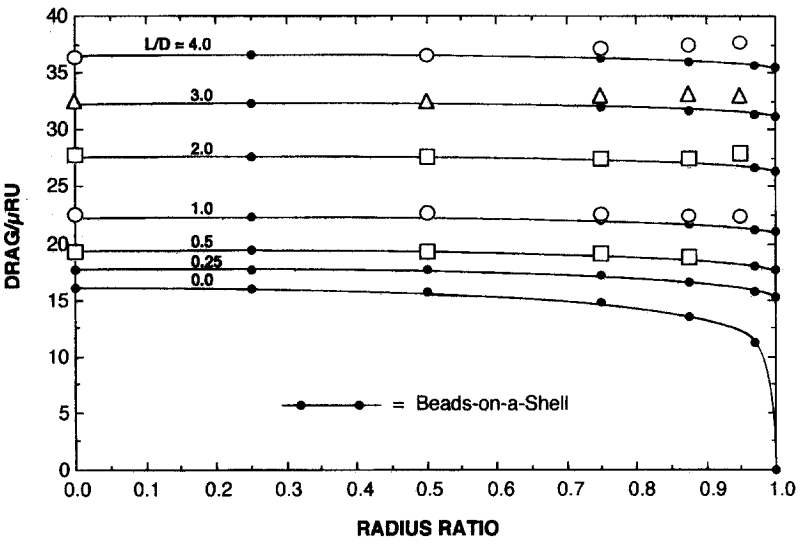

Fig. 12. – Measured and computed values of the normalized drag for hollow cylinders as a function of the radius ratio with L/D as a parameter.

where $A = L/D$ and D_0 is the nondimensional drag at A_0. The local slope of the drag curve $\partial D/\partial A$ at A_0 was determined experimentally by a least-squares fit through the measured data. The results in Figure 12 show

a continuously increasing disparity between numerical computation and laboratory measurement as L/D and R_i/R approach their largest values; the maximum 4% error occurs for the tallest $L/D = 3.81$ and the thinnest $R_i/R = 0.95$ cylinder. As noted in (Lasso and Weidman, 1986) the *ad hoc* correction procedure is designed for nearly axisymmetrical bodies of O (1) aspect ratio and is not meant to apply at large L/D where bodies appear slender as opposed to spherical. The additional breakdown as $R_i/R \rightarrow 1$ might also have been anticipated as the *ad hoc* procedure is based on an "equivalent" sphere drag and does not account for significant flow through the porous body; the data for $R_i/R = 0.95$ in Figure 12 suggests that the drag contribution due to the throughflow cannot be neglected in this limit, but we cannot verify this fact without detailed velocity distributions inside the hollow cylinder. The numerical computations, on the other hand, do account for drag contributions from both the internal and the external flow, and are accurate to 0.1%.

5. Conclusion

The Beads-on-a-Shell (BoS) technique for determining the Stokes drag on an object uniformly translating in an infinite fluid has been applied to the class of finite rigid hollow cylinders with aspect ratios $0 \leq L/D \leq 20$ and radius ratios $0 \leq R_i/R \leq 1.0$. Agreement with the measurements of (Lasso and Weidman, 1986) and with new measurements at $R_i/R = 0.95$ is very good, except at the highest values of L/D and R_i/R where their *ad hoc* correction procedure breaks down. Those adopting the *ad hoc* correction procedure introduced in (Lasso and Weidman, 1986) should be cautioned that it becomes noticeably inaccurate when $L/D > 4$, approximately.

New Stokes drag computations have also been computed and compared with previous analytical results for the cylindrical shell and the spherical shell with opposing end caps removed. The analytical predictions for the spherical shell results of (Davis, 1985) are verified by the BoS method. In the range where the analytical results for the cylindrical shell are applicable, the BoS method corroborates the predicted asymptotic Stokes drag results of (Price, 1985).

Acknowledgements.

We are grateful to K. Rupp for careful machining of the thin-walled hollow cylinders and to P. Rouse for assistance in the experiments. Dow Corning Corporation donated the silicone oil test fluid used in the experiments. This work was written up while author PDW was on sabbatical leave. He extends his gratitude to École Polytechnique for supporting a six months visit to the Laboratoire d'Hydrodynamique in Palaiseau, France and to the Spanish Ministry of Education and Culture for a three month visit to Escuela Técnica Superior de Ingenieros Aeronáuticos in Madrid, Spain under contract number SAB95-0514.

REFERENCES

AMARAKOON A. M. D., HUSSEY R. G., GOOD B. J., GRIMSAL E. G., 1982, Drag measurements for axisymmetric motion of a torus at low Reynolds number, *Phys. Fluids*, **25**, 1495-1501.

BATCHELOR G. K., 1970, Slender-body theory for particles of arbitrary cross-section in Stokes flow, *J. Fluid Mech.*, **44**, 419-440.

BLUMBERG P. N., MOHR C. M., 1968, Effect of orientation on the settling characteristics of cylindrical particles, *AIChe J.*, **14**, 331-334.

BROERSMA S., 1960, Viscous force constant for a closed cylinder, *J. Chem. Phys.*, **32**, 1632-1635.

BURGERS J. M., 1938, in Second Report on Viscosity and Plasticity of the Amsterdam Academy of Sciences, Nordemann, New York, Chap. 3.

CICHOCKI B., FELDERHOF B. U., HINSEN K., WAJNRYB E., BLAWZDZIEWUCZ J., 1994, Friction and mobility of many spheres in Stokes flow, *J. Chem. Phys.*, **100**, 3780-3790.

CICHOCKI B., HINSEN K., 1995, Stokes drag on conglomerates of spheres, *Phys. Fluids*, **7**, 285-291.

COX R. G., 1970, The motion of long slender bodies in a viscous fluid. Part I. General theory, *J. Fluid Mech.*, **44**, 791-810.

DAVIS A. M. J., 1985, Axisymmetric Stokes flow past a spherical hollow boundary and concentric sphere, *Quart. J. Mech. Appl. Math.*, **38**, 537-559.

DAVIS A. M. J., 1991, Slow viscous flow due to the motion of an annular disk; pressure driven extrusion through an annular hole in a wall, *J. Fluid Mech.*, **231**, 51-71.

DE LA TORRE J., BLOOMFIELD, V. A., 1981, Hydrodynamic properties of complex, rigid, biological macromolecules: theory and applications, *Quart. Rev. Biophys.*, **14**, 81-139.

DE MESTRE N. J., 1973, Low-Reynolds-number fall of slender cylinders near boundaries, *J. Fluid Mech.*, **58**, 641-656.

GLUCKMAN M. J., WEIBAUM S., PFEFFER R., 1972, Axisymmetric slow viscous flow past an arbitrary convex body of revolution, *J. Fluid Mech.*, **55**, 677-709.

HEISS J. F., COULL J., 1952, The effect of orientation and shape on the settling velocity of non-isosymmetric particles in a viscous medium, *Chem. Eng. Prog.*, **48**, 133-140.

KELLER J. B., RUBINOW S. I., 1976, Slender-body theory for slow viscous flow, *J. Fluid Mech.*, **75**, 705-714.

LADD A. J. C., 1988, Hydrodynamic interactions in a suspension of spherical particles, *J. Chem. Phys.*, **88**, 5051-5063.

LADD A. J. C., 1989, Hydrodynamic interactions and the viscosity of suspensions of freely moving spheres, *J. Chem. Phys.*, **90**, 1149-1157.

LADD A. J. C., 1990, Hydrodynamic transport coefficients of random dispersions of hard spheres, *J. Chem. Phys.*, **93**, 3484-3494.

LASSO I. A., WEIDMAN P. D., 1986, Stokes drag on hollow cylinders and conglomerates, *Phys. Fluids*, **29**, 3921-3934.

MAJUNDAR S. P., O'NEILL M. E., 1977, On axisymmetric Stokes flow past a torus, *Z. Angew. Math. Phys.*, **28**, 541-550.

OSEEN C. W., 1927, in Neuere Methoden Und Ergebnisse In Du Hydrodynamik, HILB E. Ed., Akademische Verlagsgesellschaft, Leipzig, Vol. 1, 25.

PRICE T. C., 1985, Axisymmetric flow past a finite circular pipe, *J. Appl. Math. Phys.*, **36**, 346-357.

RICHARDSON S., 1977, Axisymmetric slow viscous flow about a body of revolution whose section is a cardioid, *Quart. J. Mech. Appl. Math.*, **30**, 369-374.

ROGER R. P., HUSSEY R. G., 1982, Stokes drag on a flat annular ring, *Phys. Fluids*, **25**, 915-922.

ROTNE J., PRAGER S., 1969, Variational treatment of hydrodynamic interaction in polymers, *J. Chem. Phys.*, **50**, 4831-4837.

RUSSEL W. B., HINCH E. J., LEAL L. G., TIEFFENBRUCK G., 1977, Rods falling near a vertical wall, *J. Fluid Mech.*, **83**, 273-287.

SAMPSON R. A., 1891, On Stokes current function, *Phil. Trans. R. Soc. Lond.*, **A182**, 449-518.

SUTTERBY J. L., 1973, Falling sphere viscometry I. Wall and inertial corrections to Stokes law in long tubes, *Trans. Soc. Rheol.*, **17**, 559-573.

SWANSON J. E., TELLER D., DE HAEN C., 1978, The low Reynolds number translational friction of ellipsoids, cylinders, dumbbells, and hollow spherical caps. Numerical testing of the validity of the modified Oseen tensor in computing the friction of objects modeled as beads on a shell, *J. Chem. Phys.*, **68**, 5097-5102.

TELLER D. C., SWANSON E., DE HAEN C., 1979, The translational friction coefficient of proteins, in *Methods In Enzymology*, Hirs C. H. W., S. N. Timasheff Eds., Academic, New York, Vol. 61, 103-124.

UI T. J., HUSSEY R. G., ROGER R. P., 1984, Stokes drag on a cylinder in axial motion, *Phys. Fluids*, **27**, 787-795.

WAKIYA S., 1980, Axisymmetric Stokes flow about a body made of intersections of two spherical surfaces, *Arch. Mech.*, **32**, 809-817.

YAMAKAWA H., 1970, Transport properties of polymer chains in dilute solution, *J. Chem. Phys.*, **53**, 436-443.

YOUNGREN J. G. K., ACRIVOS A., 1975, Stokes flow past a particle of arbitrary shape: A numerical method of solution, *J. Fluid Mech.*, **69**, 377-403.

(Manuscript received July 7, 1997;
revised November 11, 1997.)